THE JOURNAL OF BIOLOGICAL CHEMISTRY Vol. 279, No. 14, Issue of April 2, pp. 14001–14008, 2004
Printed in U.S.A.

Structural Insight into Arginine Degradation by Arginine Deiminase, an Antibacterial and Parasite Drug Target*

Received for publication, December 8, 2003, and in revised form, December 22, 2003
Published, JBC Papers in Press, December 30, 2003, DOI 10.1074/jbc.M313410200

Andrey Galkin‡, Liudmila Kulakova§, Elif Sarikaya‡, Kap Lim‡, Andrew Howard¶‖, and Osnat Herzberg‡**

From the ‡Center for Advanced Research In Biotechnology, University of Maryland Biotechnology Institute, Rockville, Maryland 20850, §Laboratory of Parasitic Diseases, NIAID, National Institutes of Health, Bethesda, Maryland 20892-0425, ¶Advanced Photon Source, Argonne National Laboratory, Argonne, Illinois 60439, and ‖Illinois Institute of Technology, Chicago, Illinois 60616-3793

L-Arginine deiminase (ADI) catalyzes the irreversible hydrolysis of arginine to citrulline and ammonia. ADI is involved in the first step of the most widespread anaerobic route of arginine degradation. ADI, missing in high eukaryotes, is a potential antimicrobial and antiparasitic drug target. We have determined the crystal structure of ADI from *Pseudomonas aeruginosa* by the multiwavelength anomalous diffraction method at 2.45 Å resolution. The structure exhibits similarity to other arginine-modifying or substituted arginine-modifying enzymes such as dimethylarginine dimethylaminohydrolase (DDAH), arginine:glycine amidinotransferase, and arginine:inosamine-phosphate amidinotransferase, despite the lack of significant amino acid sequence homology to these enzymes. The similarity spans a core domain comprising five ββαβ motifs arranged in a circle around a 5-fold pseudosymmetry axis. ADI contains an additional α-helical domain of novel topology inserted between the first and the second ββαβ modules. A catalytic triad, Cys-His-Glu/Asp (arranged in a different manner from that of the thiol proteases), seen in the other arginine-modifying enzymes is also conserved in ADI, as well as many other residues involved in substrate binding. Based on this conservation pattern and the assumption that the substrate binding mode is similar to that of DDAH, an ADI catalytic mechanism is proposed. The main players are Cys-406, which mounts the nucleophilic attack on the carbon atom of the guanidinium group of arginine, and His-278, which serves as a general base.

L-Arginine is used by a number of microorganisms to generate ATP fermentatively by the arginine dihydrolase (ADH)[1] pathway (1, 2). First, arginine is deiminated by arginine deiminase (ADI; EC 3.5.3.6). The resulting citrulline is converted to carbamoyl phosphate and ornithine by ornithine transcarbamylase (EC 2.1.3.3), and finally the carbamoyl phosphate is used to phosphorylate ADP by carbamate kinase (EC 2.7.2.2), producing one ATP molecule (Fig. 1).

To date, ADH genes have been identified and sequenced mostly in bacteria and Archaea, and no ADH genes or ADH enzyme activity has been reported for higher eukaryotes (1). However, some amitochondriate parasitic protists such as *Trichomonas vaginalis*, *T. fetus*, *Hexamita inflate*, and one of the most commonly transmitted intestinal pathogens, *Giardia intestinalis*, have been shown to use the ADH pathway (2, 3). Recently, the first two proteins of the ADH pathway, ADI and OCT, were shown to be among 16 immunodominant proteins in *Giardia*, underscoring the importance of the ADH pathway in this parasite (4). Preliminary results from ADI gene silencing experiments in *G. intestinalis* using an RNAi construct did not yield viable organisms, suggesting that ADI plays an essential role in this pathogen.[2] Moreover, ADI competes with human nitric oxide synthase by scavenging arginine from the intestinal environment. Therefore, nitric-oxide synthesis in the intestinal epithelium, used as a host defense mechanism against microbial infection, can be blocked by ADI (4, 5).

The genetic organization of the ADH gene cluster is now known for many organisms. The structure and regulation of the operon encoding the ADH pathway have been most thoroughly studied in *Pseudomonas aeruginosa* (6–8). Pathogenic strains of this Gram-negative bacterium primarily infect immunocompromised patients, such as those suffering from burns, cystic fibrosis, and AIDS, and those undergoing chemotherapy (9). *P. aeruginosa* is a leading source of hospital-acquired infections, and it is the cause of lung damage that results in a high mortality rate of cystic fibrosis patients. The ADH pathway provides the major route of arginine catabolism in this organism and is, therefore, important for the survival and propagation of *P. aeruginosa*. The pathway is activated under anaerobic conditions and in the presence of extracellular arginine (7, 10).

The absence of the ADI gene in the human genome, together with its important function in both pathogenic protozoa and bacteria make the enzyme an attractive therapeutic drug target for the treatment of bacterial and parasitic infections. Moreover, interest has increased in ADI as a potential agent of anti-angiogenesis (11) as well as anti-leukemic and non-leukemic murine tumors (12).

We present here the crystal structure of ADI from *P. aeruginosa*. Structural similarity to a number of arginine-modifying

* This work was supported by National Institutes of Health Grant P01 GM57890. The costs of publication of this article were defrayed in part by the payment of page charges. This article must therefore be hereby marked "*advertisement*" in accordance with 18 U.S.C. Section 1734 solely to indicate this fact.

The atomic coordinates and structure factors (code 1RXX) have been deposited in the Protein Data Bank, Research Collaboratory for Structural Bioinformatics, Rutgers University, New Brunswick, NJ (http://www.rcsb.org/).

** To whom correspondence should be addressed: Center for Advanced Research in Biotechnology, 9600 Gudelsky Dr., Rockville MD 20850. Tel.: 301-738-6245; Fax: 301-738-6255; E-mail: osnat@carb.umbi.umd.edu.

[1] The abbreviations used are: ADH, arginine dihydrolase; ADI, arginine deiminase; DDAH, dimethylarginine dimethylaminohydrolase; PDB, Protein Data Bank; AGAT, arginine:glycine amidinotransferase; IPAT, arginine:inosamine-phosphate amidinotransferase.

[2] T. Nash, personal communication.

or substituted arginine-modifying enzymes provides the framework for proposing a reaction mechanism for ADI.

MATERIALS AND METHODS

Protein Production—The ADI gene from *P. aeruginosa* PAO1 was amplified using *PfuTurbo* DNA polymerase (Stratagene), genomic DNA (ATCC 47085D), and 5′ and 3′ end primers. The forward primer is 5′-CACCCTGGTGCCGCGCGGCAGC*CATATG*AGCACGGAAAAAAC-CAAACTT-3′, and the reverse is 5′-TCAGTAGTCGATCGGGTCGC-3′. In the forward primer, the sequence encoding a thrombin cleavage site is underlined, and an NdeI restriction site is shown in italic. The PCR product was introduced into pET100/D-TOPO expression vector by the TOPO directional cloning procedure (Invitrogen). Recombinant plasmids were isolated from *Escherichia coli* TOP10 strain (pET100/ADIh). An expression construct (pET100/ADIn) for the production of native protein without the His tag was prepared by digestion with NdeI and self-ligation.

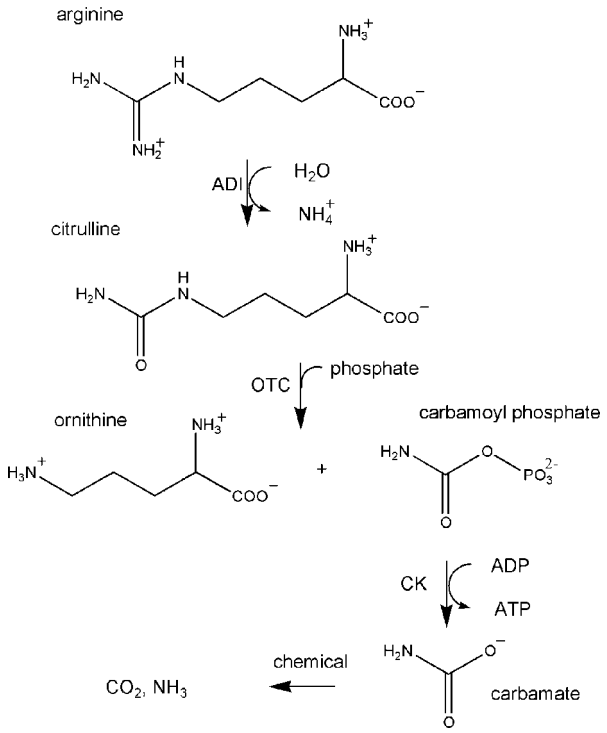

FIG. 1. **Arginine dihydrolase pathway.** *OTC*, ornithine transcarbamylase; *CK*, carbamate kinase.

For production of the selenomethionine-containing protein, the *E. coli* strain B834(DE3) was transformed with the pET100/ADIh recombinant plasmid. Minimum Eagle's medium was supplemented with ampicillin and selenomethionine. Cells were grown at 30 °C to 0.5 A_{600} when 0.1 mM isopropyl-1-thio-β-D-galactopyranoside was added for protein expression. After 4 h the cells were collected by centrifugation and suspended in 20 mM Tris-HCl buffer (pH 8.0), 0.5 M NaCl, and 5 mM imidazole. Then, cells were broken by passage through a French press. The soluble fraction was separated by centrifugation at 40,000 × *g* for 30 min and applied on a nickel-nitrilotriacetic acid metal affinity column (Qiagen). Protein was eluted with 20 mM Tris-HCl (pH 8.0), 0.5 M NaCl, and 250 mM imidazole. To remove the N-terminal sequence containing the His_6 tag, thrombin was added at a 1:2000 molar ratio and left for 2 h at room temperature in a solution of 50 mM Tris-HCl buffer (pH 8.0) and 150 mM NaCl. Thrombin was removed by passing the solution through a benzamidine column (Amersham Biosciences). Cleaved protein was separated from intact protein and from the N-terminal peptide on a second nickel-nitrilotriacetic acid column. The protein was further purified by ion-exchange chromatography on a Source 15 Q column (Amersham Biosciences). Fractions containing protein were collected and dialyzed against 50 mM Tris-HCl (pH 7.5) and 50 mM NaCl. Finally, the protein was concentrated to 6 mg/ml, flash-cooled in liquid nitrogen, and stored in aliquots at −80 °C. Protein integrity and purity were assessed by polyacrylamide gel electrophoresis in the presence of SDS.

Native protein was produced from *E. coli* strain BL21(DE3) transformed with the pET100/ADIn plasmid. Cells were grown in LB medium, and the protein was expressed under the same conditions as those described above. Native ADI was purified on an AKTAexplorer10 chromatographic station (Amersham Biosciences) using two major chromatographic steps: ion exchange and hydrophobic chromatography. An additional gel-filtration step was used if necessary to remove a small fraction of protein aggregates. Enzyme activity was determined according to a previously described procedure (6).

Analytical Size Exclusion Chromatography—Analytical size exclu-

TABLE I
X-ray data collection and refinement statistics

	MAD[a] experiment			
	Refinement data	Remote energy	Peak	Inflection
Data collection				
Space group	$P4_12_12$			
Cell dimension (Å)	$a = b = 114.9$, $c = 300.7$			
Wavelength (Å)	0.98400	0.96788	0.97925	0.97939
Resolution range (Å)	20–2.45	30–2.6	30–2.8	30–2.9
No. observations	829,494	291,943	302,165	246,607
No. unique reflections	74,771	102,813	92,639	80,262
Completeness (%)[b]	99.9 (100)	87.4 (62.7)	96.2 (84.6)	94.0 (87.2)
R_{merge}[c]	0.096 (0.416)	0.061 (0.494)	0.061 (0.336)	0.070 (0.446)
Refinement statistics				
No. reflections	73,248			
No. residues	1630			
No. water molecules	492			
R_{cryst}[d]	0.198			
R_{free}[e]	0.264			
RMS deviation				
Bonds (Å)	0.015			
Angles (°)	1.9			
Average *B* factor (Å^2)	44.1			
Ramachandran plot (%)				
Most favored	91.2			
Allowed	8.0			
Generously allowed	0.8			
Disallowed	0.0			

[a] MAD, multiwavelength anomalous diffraction; RMS, root mean square.
[b] The values in parentheses are for the highest resolution shell.
[c] $R_{merge} = \Sigma_{hkl}\,[(\Sigma_j|I_j - \langle I\rangle|)/\Sigma_j|I_j|]$ for equivalent reflections (anomalous data separated).
[d] $R_{cryst} = \Sigma_{hkl}\,||F_o| - |F_c||/\Sigma_{hkl}\,|F_o|$, where F_o and F_c are the observed and calculated structure factors, respectively.
[e] R_{free} is computed for 3802 reflections that were randomly selected and omitted from the refinement.

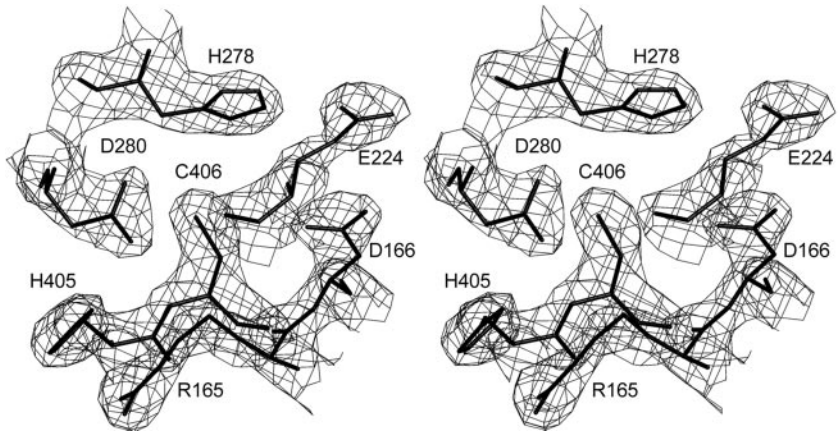

FIG. 2. **Stereoscopic view of the $2F_o - F_c$ 2.45-Å resolution electron density around the active site.** The ADI catalytic triad is formed by the residues Cys-406, His-278, and Glu-224. The map is countered at the 1σ level.

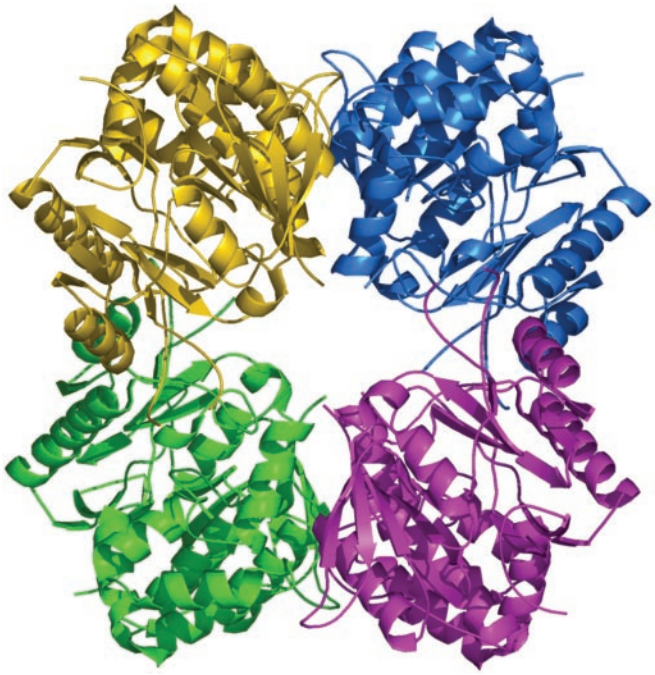

FIG. 3. **Ribbon diagram representation of the ADI tetramer.**

TABLE II
ADI structural homologs

PDB ID code	Protein name	*Z*-score	RMSD[a]	Aligned residues	Sequence identity
			Å		%
SSM program search					
1H70	DDAH	10.6	1.9	232	15
1BWD	IPAT	10.9	2.0	245	17
4JDW	AGAT	9.1	2.3	254	16
DALI program search					
1H70	DDAH	26.0	2.3	250	16
1JDW	AGAT	26.4	2.9	281	16
1BWD[b]	IPAT	26.5	2.8	278	16

[a] RMSD, root-mean-square deviation.
[b] The automatic DALI search did not identify IPAT as a structural homologue, and the result listed in the table was obtained by pairwise search of the ADI and 1BWD coordinates.

sion chromatography was performed on an AKTAexplorer10 chromatography work station, using a Superdex-200 HR 10/30 column (Amersham Biosciences). Runs were performed at 0.4 ml/min in a solution containing 50 mM Tris-HCl buffer (pH 7.5) and 0.1 M NaCl.

Crystallization and Data Collection—Selenomethionine-containing crystals were obtained in hanging drops using the vapor diffusion method at room temperature. The protein solution was mixed with an equal volume of mother liquor containing 33% 2-methyl-2,4-pentanediol, 6% polyethylene glycol 3350, 0.1 M Tris-HCl (pH 7.6), and 4% acetone, and equilibrated against the mother liquor reservoir. Crystals appeared within 6–8 days and grew to ~0.15 × 0.15 × 0.2 mm. These crystals were obtained under different conditions, have different cell parameters, and exhibit better diffraction quality than those reported previously (13).

Diffraction data for crystals produced from selenomethionine-containing protein were acquired at the Industrial Macromolecular Crystallography Association Collaborative Access Team's (IMCA-CAT) 17-ID beamline at Advanced Photon Source (APS, Argonne National Laboratory, Argonne, IL). For data acquisition, the IMCA-CAT beamline was equipped with a Quantex210 charge-coupled device detector. Data processing was carried out using HKL2000 software (14). The solvent occupies 55% of the crystal volume, and the asymmetrical unit contains four protein molecules. The statistics of data collection are provided in Table I.

Structure Determination and Refinement—The computer program SHELXD (15) was used to determine selenium sites at a resolution of 3.0 Å. Phase determination and phase improvement were carried out with the Solve/Resolve programs (16). The quality of the initial phase set was improved by density modification and extended to a resolution of 2.6 Å. The resulting electron density map revealed a 2-fold non-crystallographic symmetry axis and two other symmetry axes with translational components, relating four independent molecules in asymmetrical units to one another. Four-fold averaging produced an interpretable electron density map. The polypeptide chain of one molecule was built on a silicon graphics octane work station using the interactive computer graphics program "O" (17). After adding the side chains, the remaining molecules in the asymmetrical unit were generated by applying the non-crystallographic symmetry operators.

Structure refinement was carried out using the CNS program (18) with all data between 20 and 2.45 Å. The four molecules in the asymmetrical unit were refined independently. The resulting model was inspected and modified on a graphics work station using "O" software. In the final stages of the refinement, water molecules were added to the model based on an electron density map difference of $F_o - F_c$ (where F_o and F_c are the observed and calculated structure factors, respectively), using peaks with density $\geq 3\sigma$ as the acceptance criterion. Structure analysis was carried out using a number of computer programs, including PROCHECK for analysis of geometry (19), Quanta for solvent-accessible surface area calculations (Molecular Simulations, Inc.), DALI (20) and SSM (21) for identifying structural homologues, and PyMOL for depiction of the structure (22).

Modeling—Molecular modeling was carried out with the QUANTA2000/CHARMM26 software package (Molecular Simulations, Inc.). The citrulline ligand was extracted from the dimethylarginine dimethylaminohydrolase (DDAH) structure (Protein Data Bank (PDB) code 1H70) and placed in the active site of ADI based on the superimposition of the two structures. The arginine ligand was placed manually in a position equivalent to that of citrulline. The salt bridge between Arg-401 and Asp-166 was disrupted by changing the Arg-401 side chain conformation using the QUANTA rotamer library. The model was optimized in QUANTA by energy minimization of the arginine substrate and the surrounding residues.

RESULTS AND DISCUSSION

Structure Quality—The refinement results are summarized in Table I. The electron density map in the vicinity of the active

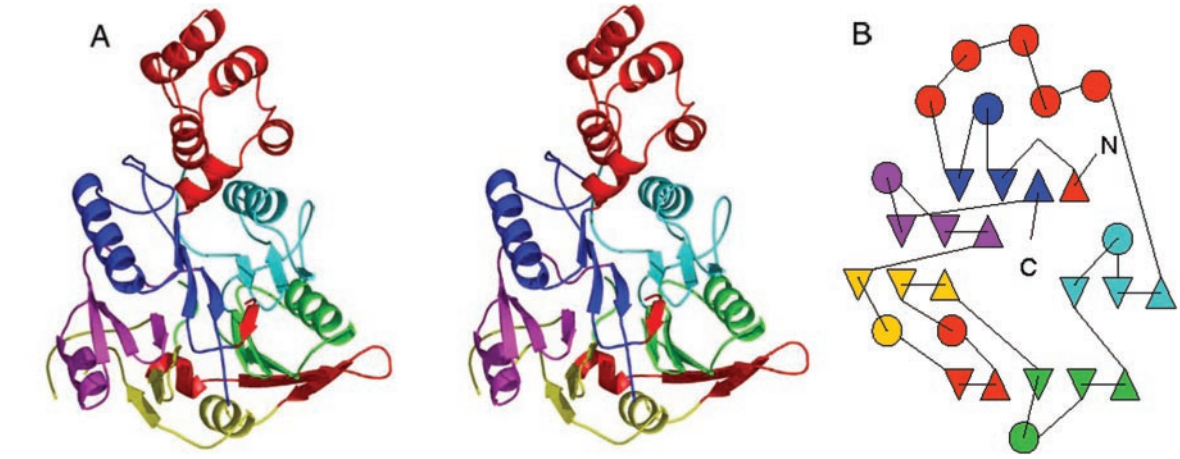

C

```
                 βI1′      βI2                                                                  αI
ADI   (6)    -TKLGVHSEAGKLRKVMVCSPGLAHQ-------------------------RLTPSNCDELLFD---DVIWVNQAKRDHFDFVTKMRERG
DDAH  (0)    ----------FMFKHIIARTPARSLVD-------------------------------GLTSSHLGKPDYAKALEQHNAYIRALQTCD
AGAT  (87)   -CPVSSYNEWDPLEEVIVGRAENACVPPFTIEVKANTYEKYWPFYQKQGGHYFP--------------KDHLKKAVAEIEEMCNILKTEG
IPAT  (1)    RSLVSVHNEWDPLEEVIVGTAVGARVPTADRSVFAVEYAGDYESQEQIPSGAYP--------------DRVLKETEEELHVLAAELTKLG

                 βI3     α′1        α′2                 α′3          α′4                 α′5
ADI   (67)   IDVLEMHNLLTETIQNPEALKWILDRKITADSVGLGLTSELRSWLESLEPRKLAEYLIGGVAADDLPASEGANILKMYREYLGHSSFLLP
DDAH  (47)   VDITLLP-----------------------------------------------------PDER----------------------------
AGAT  (139)  VTVRRPD-----------------------------------------------------PIDWS--------------------------LK
IPAT  (78)   VTVRRPG-----------------------------------------------------PRDHS--------------------------AL

                                 βII1   βII2                 αII                βII3
ADI   (157)  --------PLPNTQFTRDTTCWIYGGVTLNPMYWPARRQETLLTTAIYKFHPEFANAEFEIWYGDPDKDHG------------------
DDAH  (58)   ---------FPDSVFVEDPVLCTSRCAIITRPGAESRRGETEIIEETVQRF---Y--PGKVERIE--A----------------------
AGAT  (153)  YKTPDFESTGLYSAMPRDILIVVGNEIIEAPMAWRSRFFEYRAYRSIIKDYFH---RGAKWTTAP--KPTMADELYNQDYPIHSVEDRHK
IPAT  (91)   IKTPDWETDGFHDYCPRDGLLSVGQTIIETPMALRSRFLESLAYKDLLLEYF---ASGSRWLSAP--KPRLTDDSYA--PQA----PAG-

                          *    βIII1    βIII2              αIII               βIII3        *    βIV1    βIV2  α′6
ADI   (220)  ------------SSTLEGGDVMPIGNGVVLIGMGERSSRQAIGQVAQSLFAKGAAERVIVAGLP-KAAMHLDTVFSFCDRDLVTVFPEVV
DDAH  (110)  ------------PGTVEAGDIMMVG-DHFYIGESARTNAEGARQMIAILEK--HGLSGSVVRL--EKVLHLKTGLAYLEH1NLLAAGEFV
AGAT  (238)  LAAQGKFVTTEFEPCFDAADFIRAG-RDIFAQRSQVTNYLGIEWMRRHLA--P-DYRVHIISFKDPNPMHIDATFNIIGPGIVLSNPDRP
IPAT  (169)  ------ERLTDEEPVFDAANVLRFG-TDLLYLVSDSGNELGAKWLQSAVG--D-TYTVHPCRKL-YASTHVDSTIVPLRPGLVLTNPSRV

                 βIII4′          βIII5′      αIV          βIV3                                  βV1    βV2
ADI   (299)  KEIVPFSLRPDPSSPYGMNIRREEKTFLEVVAESLGLKKLRVVETGGNSFEREQWD--------------DGNNVVCLEPGVVVGYDRNT
DDAH  (183)  SK----------------------PEFQ---------DFNIIEIPE-----EE---------------SYAANCIWVN-ERVIMPAGYP
AGAT  (324)  CH----------------------QIDLFKKA-----GWTIITPPT-----PIIPDDHPL---WMSSKWLSMNVLMLDEKRVMVDANEV
IPAT  (248)  NDEN--------------------MPDFLR-------SWENITCPE-----LVDI--GFTGDKPHCSVWIGMNLLVVRPDLAVVDRRQT

                 αV        βV3                 *   βI1
ADI   (377)  YTNTLLRKAGVEVITISASELGRGRGGGHCMTCPIVRDPID
DDAH  (220)  RTREKIARLGYRVIEVDTSEYRKIDGGVSCMSLRF
AGAT  (378)  PIQKMFEKLGITTIKVNIRNANSLGGGFHCWTCDVRRGTLQSYLD
IPAT  (303)  ALIRLLEKHGMNVLPLQLTHSRTLGGGFHCATLDVRRTGALETYQF
```

FIG. 4. **Overall fold, topology, and structure-based sequence alignment of ADI.** *A*, stereoscopic view of the fold in an orientation that highlights the 5-fold pseudosymmetry with the five modules depicted in different colors. *Blue*, I (residues 6–71 and 409–417); *cyan*, II (residues 158–227); *green*, III (residues 228–282); *yellow*, IV (residues 283–301 and 321–361); and *magenta*, V (residues 362–408). The unique ADI α-helical domain (residues 72–157), the additional β strand of module I (residues 8–10), and the two additional β strands of the module III (residues 302–308 and 316–320) are shown in *red*. *B*, topological diagram of the secondary structure elements of ADI; *triangles*, β strands; *circles*, α-helices. The coloring scheme is the same as in *A*. *C*, structure-based sequence alignment of ADI, DDAH (PDB code 1H70), AGAT (PDB code 4JDW), and IPAT (PDB code 1BWD). *Roman numerals* are used for the ββαβ modules. β strands and α-helices are colored *blue* and *red*, respectively. β strands within ββαβ modules are numbered sequentially. Secondary structures units outside the modules are indicated by a *prime character* and are numbered sequentially. The catalytic triad residues are marked with an *asterisk*.

side is shown in Fig. 2. There are four protein molecules in the asymmetrical unit, A, B, C, and D, containing a total of 1630 amino acid residues and 492 water molecules. The monomers exhibit root-mean-square deviations of α-carbon positions in the range 0.2–0.7 Å. The five N-terminal residues of each molecule are not visible in the electron density map. In addition, no electron density is associated with the protein surface residues 249, 250, 273, 274, and 418 in molecule A, 151, 152, 273, 274, and 347–351 in molecule B, 352 in molecule C, and 273, 274, 345–352, and 418 in molecule D. They were omitted from the final model.

Overall Structure—ADI from *P. aeruginosa* forms tetramers with an approximate symmetry of 222. The packing is mediated by two perpendicular non-crystallographic symmetry axes and a crystallographic axis (Fig. 3). In the crystal, molecules A and B belong to one tetramer and molecules C and D to a second tetramer. The analytical gel filtration experiments show that the tetramer is the predominant form in solution as well. The buried contact surface area per monomer is 2785 Å^2, ~16% of the monomer surface area. Hydrophobic monomer contact surface area is 1029 Å^2, ~21% of the total hydrophobic surface area of the monomers.

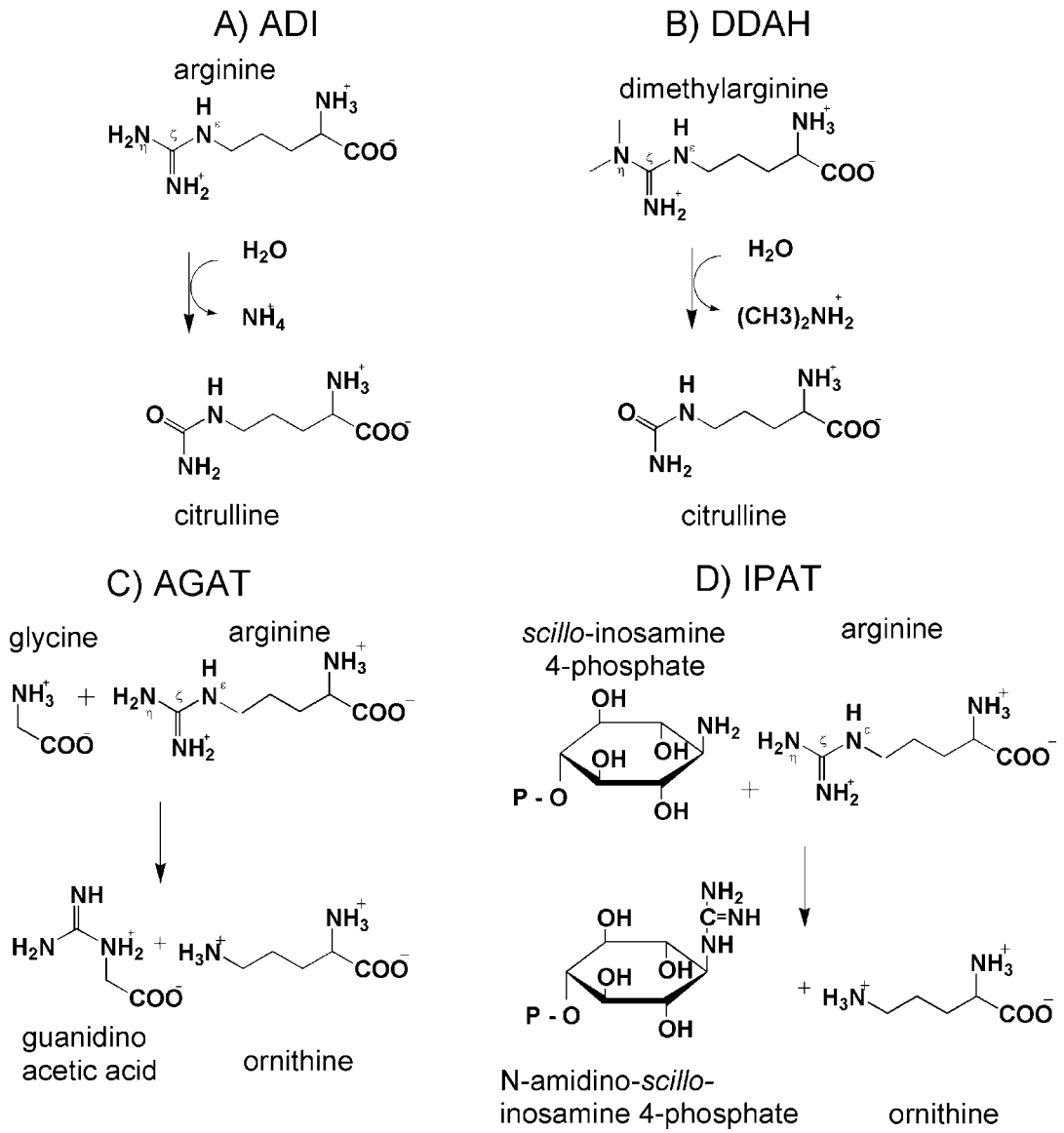

FIG. 5. **Reactions catalyzed by ADI structural homologs ADI (*A*), DDAH (*B*), AGAT (*C*), and IPAT (*D*).**

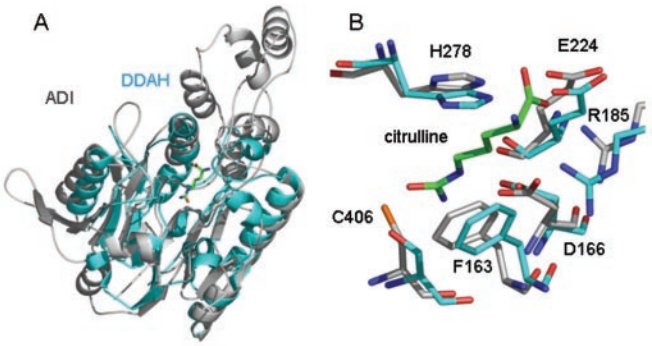

FIG. 6. **Structural relationship between ADI and DDAH.** *A*, superimposition of the ADI (*gray*) and DDAH (*cyan*) monomers. The C249S mutant DDAH in complex with citrulline (PDB code 1H70) was used. The citrulline product is shown in *green*. *B*, superimposition of the active site residues of ADI and DDAH. Colors are the same as in *A*. The residues of ADI are labeled.

The overall fold of ADI consists of five $\beta\beta\alpha\beta$ modules in cyclical arrangement, generating a pseudo 5-fold symmetrical barrel and an additional 85-residue α-helical domain inserted between the first and the second $\beta\beta\alpha\beta$ modules (Fig. 4). The three β strands in each $\beta\beta\alpha\beta$ module are arranged as a mixed β sheet, approximately parallel to the barrel pseudo 5-fold axis. As previously predicted (23, 24), the core barrel of ADI is structurally similar to DDAH (25) and to two amidinotransferases, arginine:glycine amidinotransferase (AGAT) (26) and arginine:inosamine-phosphate amidinotransferase (IPAT) (27) (Table II). Yet, the amino acid sequence identity between ADI and these proteins is low, ranging between 15 and 17%. The root-mean-square deviation values of α-carbon positions between the aligned residues of ADI and the other three proteins range between 1.9 and 2.9 Å. So far, ADI is the largest enzyme of the structural superfamily (418 *versus* ~360 residues for the amidinotransferases and 254 residues for DDAH). The 85-residue insertion is unique to ADI and includes five α-helices ($\alpha'1$–5 in Fig. 4), a short 3/10 helix, and a single short β strand (not highlighted in Fig. 4, for clarity). The automated structure comparison programs SSM (21) and DALI (20) did not reveal a significant similarity between this α-helical domain and any structure currently in the PDB. The α-helical domain mediates tetramer formation (the contact between the yellow and blue molecules and between the green and magenta molecules in Fig. 3). All other structural relatives of ADI are dimers.

Another unique feature of ADI is the β strand insertions in

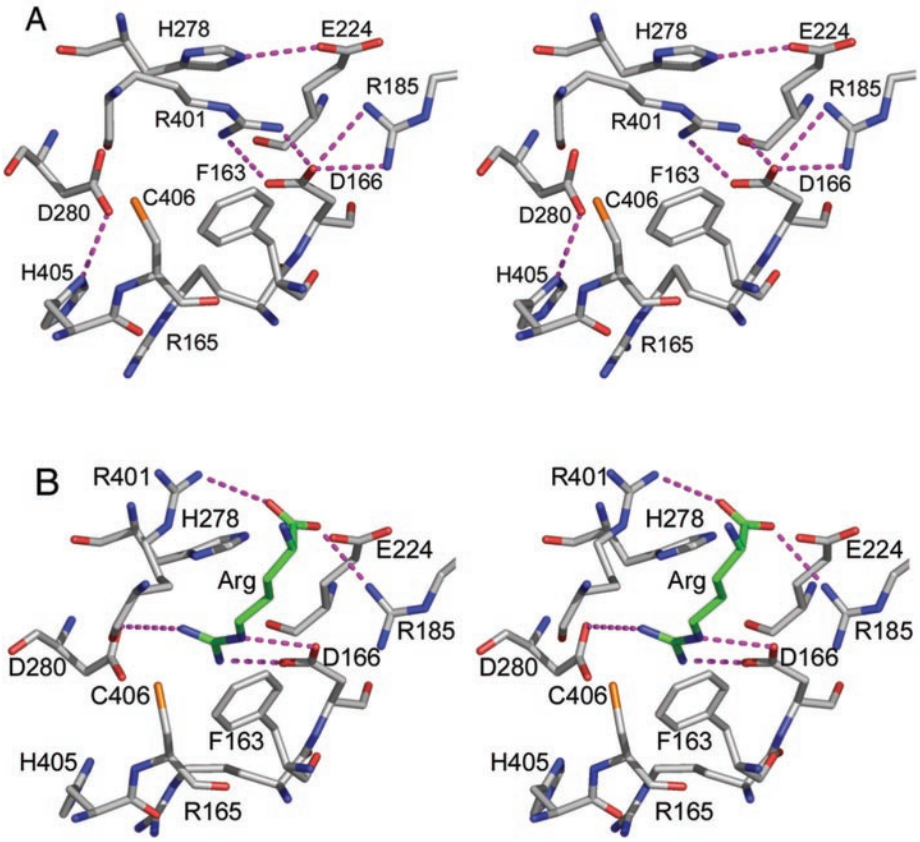

FIG. 7. **The active site architecture of ADI and proposed model of bound substrate.** *A*, a stereoscopic view of key active site residues is shown. Atomic colors are *red*, oxygen; *blue*, nitrogen; *yellow*, sulfur; and *gray*, carbon. Ion pair interactions are shown as *dashed lines*. *B*, a stereoscopic view is shown of a modeled arginine substrate (*green*) docked in the active site of ADI. The sulfur atom of Cys-406 is oriented appropriately for nucleophilic attack on the Cζ atom of the guanidinium group of arginine. The atomic colors are the same as in *A*. Charge interactions between substrate and protein groups are indicated by *dashed lines*.

the first and third $\beta\beta\alpha\beta$ modules, extending these β sheets with the topologies $\beta\beta\beta\alpha\beta$ and $\beta\beta\alpha\beta\beta\beta$, respectively (Fig. 4, *B* and *C*). The core $\beta\beta\alpha\beta$ modules are always the same; the first β strand occupies the inner most position and makes a hairpin loop connection to a second antiparallel β strand, which is in turn linked to the third parallel β strand via a crossover connection containing an α-helix, forming a mixed β sheet. However, in module I the 3-stranded β sheet is augmented with a β strand (βI1′) adjacent to the first one (βI1). In module III the β sheet is extended by two antiparallel β strands βIII4′ and βIII5′, which are inserted between the second β strand (βIV2) and the α-helix (αIV) of module IV (Fig. 4, *B* and *C*). This insertion contains a short α-helix (α′6, residues 295–298).

Active Site Architecture—The active site topology of ADI is similar to that of the other enzymes of the structural superfamily DDAH, IPAT, and AGAT. The catalytic triad Cys-His-Glu/Asp seen in the other arginine modifying enzymes is also conserved in ADI, as well as many other residues involved in substrate binding (Fig. 4*C*). Note that the special arrangement of the catalytic triad here is different from that of the well studied thiol and serine proteases (28, 29), because the cysteine and histidine residues do not interact with each other (the distance between the two is ~7 Å).

Although the two amidinotransferases (IPAT and AGAT) have the same orientation as the target scissile bond of the substrate with respect to the cysteine and histidine catalytic residues, the bond to be cleaved is different (Cζ–Nϵ *versus* Cζ–Nη). Consequently, the substrate orientation in AGAT and IPAT is different compared with that of DDAH (25, 26) and ADI. AGAT and IPAT catalyze amidinotransferase reactions in which the amidino group of arginine is transferred to a second substrate, producing the amidino derivatives of the substrates and ornithine (Fig. 5). In contrast, DDAH and ADI are hydrolytic enzymes, catalyzing the same bond cleavage (Cζ–Nη) (Fig. 5). Therefore, further comparisons were made with the structure of the C249S mutant DDAH in complex with citrulline ((25) PDB code 1H70). Superimpositions of these two structures and of six conserved active site residues, including the catalytic triad (Cys-406, His-278, and Glu-224 in ADI), are shown in Fig. 6. The nearly identical locations of these residues together with the structure-based sequence alignment support the active site assignment of ADI.

The active site of ADI is strikingly enriched with charged residues (Fig. 7*A*). It contains only one hydrophobic residue, Phe-163. The charge state of the catalytic residue, Cys-406, remains to be determined. An exquisite network of ion pair interactions ensures structural integrity and may also play a role in enzyme activity. Most of these residues are invariant in the known ADI sequences. The Asp-280 carboxylate group interacts with the imidazole group of His-405, which in turn interacts with Glu-13 (not shown). Of these three residues, Asp-280 and Glu-13 are invariant in all known ADIs, and His-405 is sometimes replaced by an arginine. An unusual feature of this network is the presence of another invariant residue, Arg-165, of which the guanidinium group stacks against the His-405 imidazole ring, and both residues are buried (Fig. 7*A*). The desposition of Arg-165 is fixed by electrostatic interactions with the main chain oxygen atoms of Thr-408 and His-405 and with the hydroxyl group of Thr-408 (not shown in the figure).

The charge network is further extended by the interaction between Glu-224 and His-278, which in turn interacts with the carboxyl group of Asp-227. The last ionic cluster involves Asp-166, Arg-185, and Arg-401 (Fig. 7*A*). This network is extended beyond the active site to include Glu-188 (not shown), which forms an ion pair with Arg-185.

Proposed Michaelis Complex and Catalytic Mechanism—The ADI active site is blocked because the side chain of Arg-401 forms an ion pair with the carboxyl group of Asp-166 and occupies approximately the same position as the guanidinium

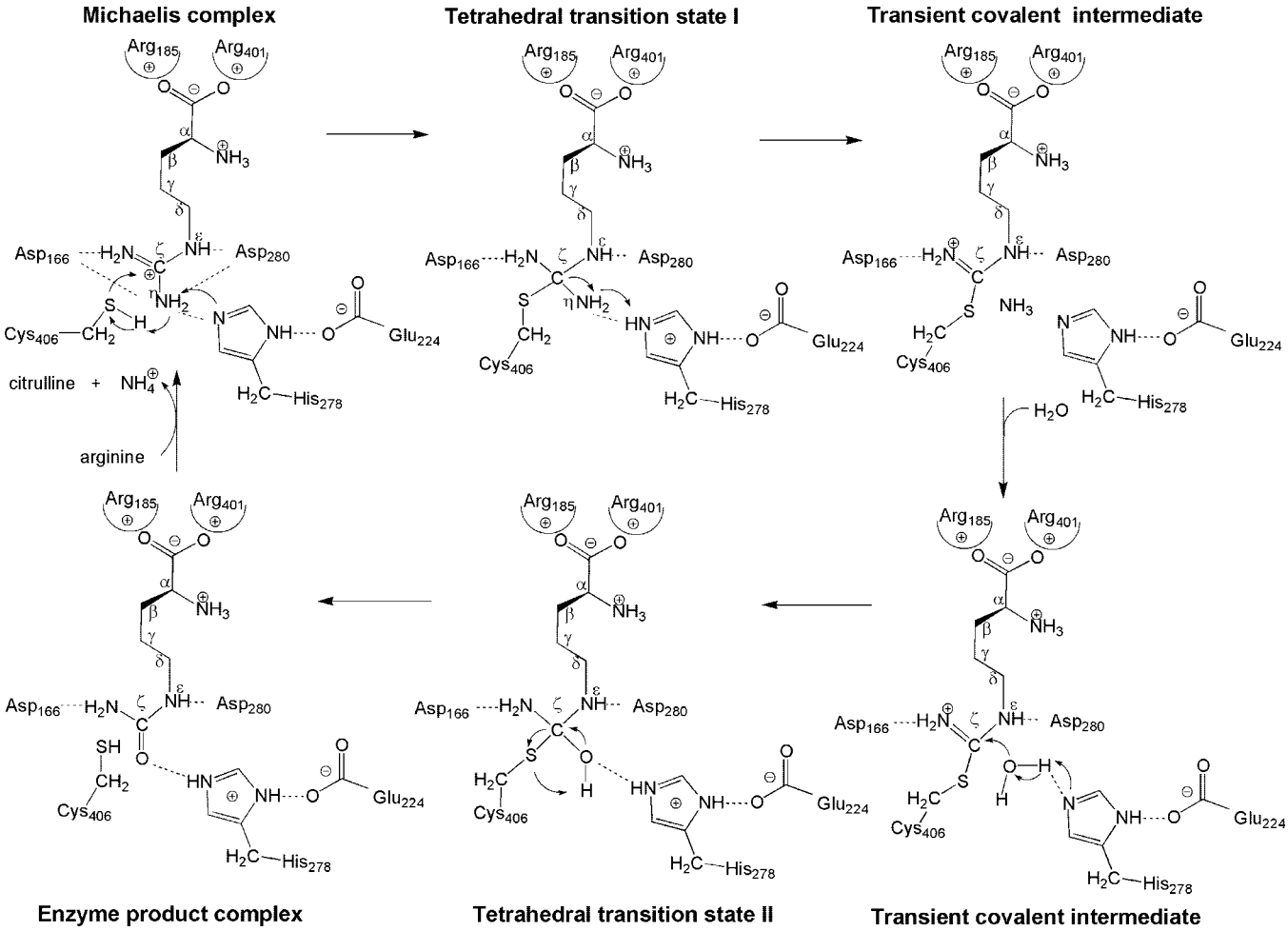

FIG. 8. **The proposed reaction mechanism of ADI.** Deimination involves the formation of two tetrahedral transition states and a transient covalent intermediate on Cys-406.

group of an arginine substrate (Fig. 7*A*). Thus, the enzyme must undergo conformational transition on substrate binding. Hindering substrate access to the active site may play a regulatory role in preventing degradation at low intracellular concentrations of arginine.

For docking, the dihedral angles of the Arg-401 side chain were modified to allow access to the binding site, and the Michaelis complex of ADI with arginine was modeled as described under "Materials And Methods." In the model, the guanidinium group of the arginine substrate is fixed tightly by interactions with the carboxyl groups of Asp-166 and Asp-280 (Fig. 7*B*). The hydrophobic part of the arginine side chain interacts with the conserved Phe-163, and its carboxyl group forms ionic interactions with Arg-185 and Arg-401. The interaction with Arg-401 is speculative, however, because the actual conformation adopted by the Arg-401 side chain is unknown. Orienting the arginine substrate in this manner places the plane of the guanidinium group between two side chains, the thiol group of Cys-406 and the imidazole group of His-278.

Based on mutagenesis studies and structural data, catalytic mechanisms for DDAH and AGAT were proposed (25, 26, 30). The overall structural similarity of DDAH, AGAT, and ADI, the conservation of the catalytic triad, and the common orientation of the scissile bond relative to the catalytic cysteine suggest a similar reaction mechanism for the three enzymes. With this consideration in mind, we propose a two-step reaction for arginine hydrolysis by ADI involving a covalent intermediate (Fig. 8). The reaction begins with binding of arginine in the active center, concomitant with swapping of the Arg-401 side chain out of the pocket. The pK_a of Cys-406 has not yet been determined, thus we do not know the ionization state of this residue in the resting state. The mechanism illustrated in Fig. 8 is written for a thiol group. If Cys-406 is ionized in the resting state, we assume that the proton would reside on Asp-280, the closest proton-accepting group to Cys-406 (3.7 Å). The Michaelis complex and the tetrahedral transition state I would change slightly, but the mechanism would be essentially the same.

The first chemical step is initiated by the nucleophilic attack of the Cys-406 thiol group on the guanidinium group Cζ atom, and concomitant proton transfers to the nitrogen atom, Nη, and from Nη to His-278 (Fig. 8). The electrophilicity of Cζ is modulated by interaction of the guanidinium group with Asp-166 and Asp-280, and His-278 serves as a general base. In turn, the ionization state of Asp-280 could be modulated by its network partners His-405, Arg-165, and Glu-13, and the ionization state of Asp-166 could be influenced by Arg-185. This first tetrahedral transition state is followed by the formation of a transient covalent intermediate and the release of ammonia after cleavage of the Cζ–Nη bond (Fig. 8). In the second step of the reaction, ammonia is replaced by a water molecule. This water molecule is activated by His-278 and attacks the Cζ atom of the covalent intermediate. Here again, His-278 serves as the general base. Finally, the carbon-sulfur bond between the enzyme and the resulting citrulline is cleaved, and free enzyme is generated for the next catalytic cycle.

It is worthwhile noting that an alternative mechanism that invokes Asp-280 as a general base instead of His-278 can also be proposed. This would imply that the unusual charge net-

work of Asp-280, His-405, Arg-165, and Glu-13 plays a major catalytic role. This network is conserved in all known ADI amino acid sequences as well as in IPAT and AGAT but is not conserved in DDAH. In contrast, His-278 is a conserved residue in all superfamily members.

In conclusion, the crystal structure of arginine deiminase and the enzyme-substrate complex model suggest further experiments to elucidate the proposed mechanism. Furthermore the ADI structure provides a framework for a rational design of new therapeutic agents against bacterial and parasitic infections.

Acknowledgments—We thank John Moult and Eugene Melamud for the use of and help with their bioinformatics web site (s2f. carb.nist. gov). We thank John Moult and Debra Dunaway-Mariano for useful discussions. We thank the staff of IMCA-CAT at the APS for help during data collection. The IMCA-CAT facility is supported by the companies of the Industrial Macromolecular Crystallographic Association through a contract with the Illinois Institute of Technology. The APS was supported by the U. S. Department of Energy, Basic Energy Sciences, Office of Science, under contract W-31-109-Eng-38. The Keck foundation provided generous support for the purchase of x-ray equipment at the Center for Advanced Research in Biotechnology.

REFERENCES

1. Zuniga, M., Perez, G., and Gonzalez-Candelas, F. (2002) *Mol. Phylogenet. Evol.* **25,** 429–444
2. Knodler, L. A., Sekyere, E. O., Stewart, T. S., Schofield, P. J., and Edwards, M. R. (1998) *J. Biol. Chem.* **273,** 4470–4477
3. Biagini, G. A., Yarlett, N., Ball, G. E., Billetz, A. C., Lindmark, D. G., Martinez, M. P., Lloyd, D., and Edwards, M. R. (2003) *Mol. Biochem. Parasitol.* **128,** 11–19
4. Palm, J. E., Weiland, M. E., Griffiths, W. J., Ljungstrom, I., and Svard, S. G. (2003) *J. Infect. Dis.* **187,** 1849–1859
5. Eckmann, L., Laurent, F., Langford, T. D., Hetsko, M. L., Smith, J. R., Kagnoff, M. F., and Gillin, F. D. (2000) *J. Immunol.* **164,** 1478–1487
6. Baur, H., Luethi, E., Stalon, V., Mercenier, A., and Haas, D. (1989) *Eur. J. Biochem.* **179,** 53–60
7. Gamper, M., Zimmermann, A., and Haas, D. (1991) *J. Bacteriol.* **173,** 4742–4750
8. Luthi, E., Mercenier, A., and Haas, D. (1986) *J. Gen. Microbiol.* **132**, 2667–2675
9. Smith, R. S., and Iglewski, B. H. (2003) *Curr. Opin. Microbiol.* **6,** 56–60
10. Lu, C. D., Winteler, H., Abdelal, A., and Haas, D. (1999) *J. Bacteriol.* **181,** 2459–2464
11. Beloussow, K., Wang, L., Wu, J., Ann, D., and Shen, W. C. (2002) *Cancer Lett.* **183,** 155–162
12. Wheatley, D. N., and Campbell, E. (2002) *Pathol. Oncol. Res.* **8,** 18–25
13. Oudjama, Y., Tricot, C., Stalon, V., and Wouters, J. (2002) *Acta Crystallogr. Sect. D Biol. Crystallogr.* **58,** 2150–2152
14. Otwinowski, Z., and Minor, W. (1997) *Methods Enzymol.* **276,** 307–326
15. Schneider, T. R., and Sheldrick, G. M. (2002) *Acta Crystallogr. Sect. D Biol. Crystallogr.* **58,** 1772–1779
16. Terwilliger, T. C. (2002) *Acta Crystallogr. Sect. D Biol. Crystallogr.* **58,** 1937–1940
17. Kleywegt, G. J., and Jones, T. A. (1999) *Acta Crystallogr. Sect D Biol. Crystallogr.* **55**, 941–944
18. Brunger, A. T., Adams, P. D., Clore, G. M., DeLano, W. L., Gros, P., Grosse-Kunstleve, R. W., Jiang, J. S., Kuszewski, J., Nilges, M., Pannu, N. S., Read, R. J., Rice, L. M., Simonson, T., and Warren, G. L. (1998) *Acta. Crystallogr. Sect D Biol. Crystallogr.* **54**, 905–921
19. Laskowski, R. A., and MacArthur, M. W. (1993) *J. Appl. Crystallogr.* **26,** 283–291
20. Holm, L., and Sander, C. (1993) *J. Mol. Biol.* **233,** 123–138
21. Krissinel, E., and Henrick, K. (2003) in *Proceedings of the 5th International Conference on Molecular Structural Biology* (Kungl, A. J., and Kungl, P. J., eds) September 3–7, 2003, p. 88, Austrian Chemical Society, Vienna
22. DeLano, W. L. (2002) *The PyMOL User's Manual*, DeLano Scientific, San Carlos, CA
23. Leiper, J. M., Santa Maria, J., Chubb, A., MacAllister, R. J., Charles, I. G., Whitley, G. S., and Vallance, P. (1999) *Biochem. J.* **343,** 209–214
24. Shirai, H., Blundell, T. L., and Mizuguchi, K. (2001) *Trends Biochem. Sci.* **26,** 465–468
25. Murray-Rust, J., Leiper, J., McAlister, M., Phelan, J., Tilley, S., Santa Maria, J., Vallance, P., and McDonald, N. (2001) *Nat. Struct. Biol.* **8,** 679–683
26. Humm, A., Fritsche, E., Steinbacher, S., and Huber, R. (1997) *EMBO J.* **16,** 3373–3385
27. Fritsche, E., Bergner, A., Humm, A., Piepersberg, W., and Huber, R. (1998) *Biochemistry* **37,** 17664–17672
28. Ye, S., and Goldsmith, E. J. (2001) *Curr. Opin. Struct. Biol.* **11,** 740–745
29. Bode, W., and Huber, R. (2000) *Biochim. Biophys. Acta* **1477,** 241–252
30. Fritsche, E., Humm, A., and Huber, R. (1999) *J. Biol. Chem.* **274,** 3026–3032